Grain size dependence of elastic anomalies accompanying the α–β phase transition in polycrystalline quartz

2008 J. Phys.: Condens. Matter 20 075229

(http://iopscience.iop.org/0953-8984/20/7/075229)

J. Phys.: Condens. Matter **20** (2008) 075229 (18pp) doi:10.1088/0953-8984/20/7/075229

Grain size dependence of elastic anomalies accompanying the α–β phase transition in polycrystalline quartz

Ruth E A McKnight[1], T Moxon[1], A Buckley[1], P A Taylor[1], T W Darling[2] and M A Carpenter[1]

[1] Department of Earth Sciences, University of Cambridge, Downing Street, Cambridge CB2 3EQ, UK
[2] Department of Physics, University of Nevada, Reno, NV 89577, USA

E-mail: ream3@cam.ac.uk

Received 6 November 2007, in final form 3 January 2008
Published 31 January 2008
Online at stacks.iop.org/JPhysCM/20/075229

Abstract

The effects of grain size on the elastic properties of quartz through the α–β phase transition have been investigated by resonant ultrasound spectroscopy. It is found that there are three regimes, dependent on grain size, within which elastic properties show different evolutions with temperature. In the large grain size regime, as represented by a quartzite sample with ~100–300 μm grains, microcracking is believed to occur in the vicinity of the transition point, allowing grains to pull apart. In the intermediate grain size regime, as represented by novaculite (1–5 μm grain size) and Ethiebeaton agate (~120 nm grain size), bulk and shear moduli through the transition follow closely the values expected from averages of single crystal data. The novaculite sample, however, has a transition temperature ~7 °C higher than that of single crystal quartz. This is assumed to be due to the development of internal pressure arising from anisotropic thermal expansion. In the small grain size region, agates from Mexico (~65 nm) and Brazil (~50 nm) show significant reductions in the amount of softening of the bulk modulus as the transition point is approached from below. This is consistent with a tendency for the transition to become more second order in character. The apparent changes towards second order character do not match quantitative predictions for samples with homogeneous strain across elastically clamped nanocrystals, however. Some of the elastic variations are also due to the presence of moganite in these samples. True 'nanobehaviour' for quartz in ceramic samples thus appears to be restricted to grain sizes of less than ~50 nm.

1. Introduction

Research into nanomaterials has many driving forces, not least the development of technological devices, and the applications are impacting many areas of science including medicine, physics, earth sciences, engineering, and numerous others (e.g. Moriarty 2001, Kassing *et al* 2006). Both theoretical and experimental work have shown that materials which have previously been examined at the micron scale must now be re-examined at the nanometre scale in order to gain a full understanding of their properties, as there are often remarkable differences between the two levels (Pertsev and Salje 2000, Moriarty 2001, Ríos *et al* 2001, Kassing *et al* 2006). When grain sizes decrease to the nanometre scale, physical properties can be significantly altered from those of similar micron-sized grains. The processes responsible for these changes are believed to be caused mainly by an increase in grain-surface effects which become dominant over the bulk at the nanoscale, and also by the implementation of boundary conditions through intergrain contacts, as in ceramics, or via constraints by substrates on thin films (e.g. Ríos *et al* 2001).

Many properties of materials are highly sensitive to small changes in crystal structure which occur in the vicinity of phase transitions. Phase transitions also involve cooperative displacements of atoms over significant length scales and should themselves be sensitive to grain size. This sensitivity can be used to explore the role of grain size and grain boundary effects in ceramics. One theoretical model of

the influence of grain size on thermodynamic behaviour and physical properties across a phase transition is provided by Pertsev and Salje (2000). They modelled a polycrystalline material as an individual nanocrystal within a homogeneous matrix. In such a system the nanocrystal is clamped elastically by the surrounding matrix and is unable to deform freely because of thermal expansion of surrounding grains with different crystallographic orientations. The effect is to restrict or suppress the development of spontaneous strain. All constituent crystallites in the polycrystal can then be considered to be under the same constraints from their respective surroundings so that the bulk behaviour will be that of an elastically clamped system rather than of a free-standing crystal. The three-dimensional elastic clamping causes a change in the order of the transition with respect to a stress-free crystal by renormalization of the fourth order coefficient, b^*, in the free energy expansion. In particular, the first order transition seen in a free-standing single crystal of quartz (b^* = negative) is predicted to become second order in a polycrystal (b^* = positive). Such obvious changes in behaviour should, in principle, be straightforward to verify experimentally. However, the study of nanoceramics is somewhat limited by the techniques available to produce samples with a uniform distribution of nanosized grains. Many successful studies have been carried out using thin films (e.g. Kassing *et al* 2006), but a solid ceramic with a small grain size distribution at the nanoscale is comparatively much more difficult to synthesize.

Here we take advantage of the natural nanoceramic, agate. Agates are relatively pure (usually >97%) compact intergrowths of fine grains of silica minerals. Ríos *et al* (2001) have found that these polycrystalline agates can display significant differences in physical properties through the α–β transition in comparison with single crystal quartz. Discontinuities in unit cell parameters, specific heat capacity, excess second-harmonic intensity and excess entropy seen at the phase transition temperature for the first order transition in a single crystal of quartz become much less pronounced in the close vicinity of the transition point. This is consistent with the view of Pertsev and Salje (2000) that suppression of strain-order parameter coupling due to three-dimensional elastic clamping causes the renormalization of the fourth order Landau coefficient. Such changes, however, must also give rise to marked differences in elastic properties. While these should provide more definitive evidence for a change from first order to second order character for the transition, they have not yet been investigated. It is well known that elastic moduli show large variations in materials which undergo structural phase transitions through their dependence on the order parameter susceptibility (Rehwald 1973, Lüthi and Rehwald 1981, Fleury and Lyons 1981, Cummins 1983, Carpenter and Salje 1998). In this study we have measured the elastic properties of a selection of natural quartzite and agate samples through the α–β quartz transition with the aim of determining the influence of grain size on elastic behaviour.

Resonant ultrasound spectroscopy (RUS) is one of the most straightforward methods available for determining the elastic behaviour of a polycrystalline material as a function of temperature (Migliori *et al* 1993, 2001, Maynard 1996, Leisure and Willis 1997, Migliori and Maynard 2005). The square of the resonance frequency of any peak in a RUS spectrum scales linearly with the effective elastic modulus (or combination of moduli) associated with that vibrational mode (Migliori and Sarrao 1997), and an isotropic material only has two independent moduli, the bulk (K) and the shear (G) moduli. Variations in the quality factor, Q, which is a measure of anelastic dissipation, can also be obtained from *in situ* measurements at high temperatures. Even if the quality of spectra is relatively poor, such that absolute values of K and G are not obtained, it is still possible to use frequencies of individual peaks as indicators of changes in elastic properties with temperature. A particular advantage of this approach, when dealing with nanoquartz, is that it avoids the problems of line-broadening in diffraction experiments due to small grain size that were encountered by Ríos *et al* (2001).

The specific objectives of the present study were:

(i) To follow the elastic constant variations through the α–β phase transition as a function of grain size in bulk samples.
(ii) To test the model of Pertsev and Salje (2000) for a change from first order to second order character at small grain sizes.
(iii) To identify the critical grain size below which the elastic properties of nanoquartz are no longer the same as for macroquartz.
(iv) To examine the extent to which microcracking develops. In other words, is there a grain size above which grains pull apart but below which they remain fully coherent?

The paper is set out as follows. Section 2 contains a brief outline of the Landau theory which can be used to relate changes in bulk modulus to differences in elastic relaxation mechanisms. The natural samples and the methodology used to study them are then described in section 3. RUS data are presented and their analysis is described in section 4. Differences between observed and predicted variations in properties due to grain size effects and their implications are discussed in section 5.

2. Landau theory

Descriptions for two limiting cases: free crystals and clamped (uniform) polycrystals

The influence of grain size on the elastic properties of a polycrystalline material containing a single phase which undergoes a displacive phase transition can be analysed in terms of the interactions between an individual crystallite and the isotropic matrix within which it is enclosed (Pertsev and Salje 2000). Spontaneous strains developing in the crystallite as a consequence of the transition differ in orientation from those of the surrounding matrix, and the scientific problem becomes one of defining the stress relaxations which follow. In one limiting case, the matrix might be considered as being rigid. A simple volume strain, for example, will then cause a change in pressure within the crystallite, so that the transition temperature will be renormalized as if an external pressure

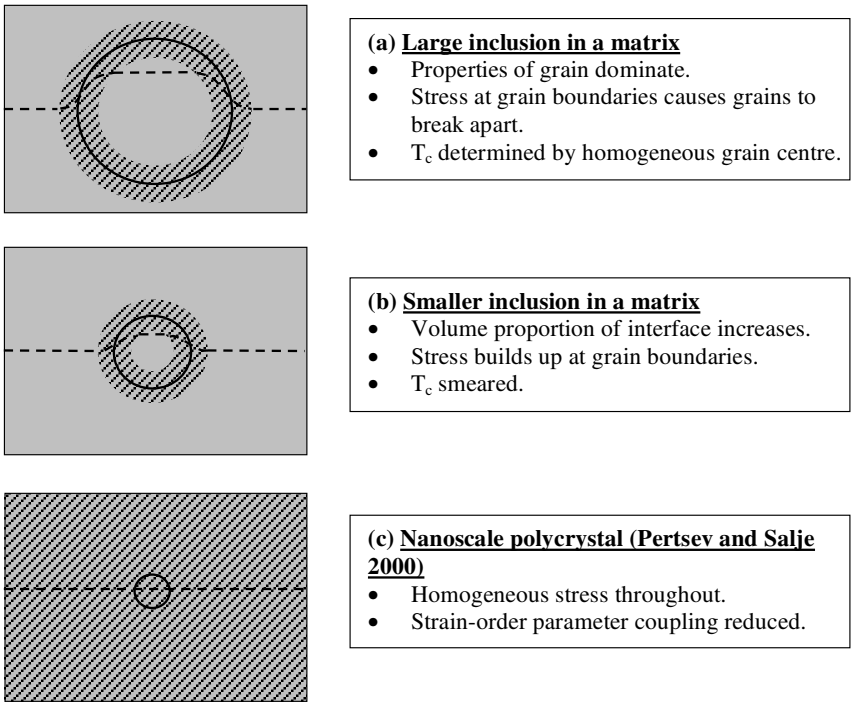

Figure 1. Cartoons to represent three different patterns of stress/strain variations through a polycrystalline material. Following Pertsev and Salje (2000), the effect of grain size is considered by treating the polycrystalline sample in terms of a single crystallite resting in a homogeneous matrix. The circles are the single crystal inclusions, which vary in size. The area surrounding the crystal is the homogeneous matrix. The hatched area represents a strain field built up at the interfaces between crystal and matrix due to the effects of differential thermal expansion. The dashed line across each figure represent the schematic variation of stress across the material. Note that the hatched strain field is relatively small in (a) with the bulk grain dominating the behaviour. The interfacial region starts to dominate as grains become smaller in (b). T_c in the interfacial region may differ from that of the bulk due to the influence of shear stress, so that the transition point of the whole sample will be smeared. At the lower limit of grain size (c), stress and strain are effectively homogeneous throughout.

had been applied to a free crystal. In reality the matrix has elastic properties which are directly related to those of the inclusion, and an abrupt stress contrast at the interface between crystallite and matrix is not sustained. Three possible relaxation mechanisms exist. Firstly, the grain boundaries might crack open, allowing grain rotations and complete stress release. Secondly, if time and temperature permit, plastic deformation or chemical diffusion in the interface region could result in an equivalent mechanical equilibration. Both these mechanisms allow the crystallite (and matrix) to evolve with the same structural parameters and physical properties as would occur in a free crystal. In the absence of complete plastic relaxation or crack development, the third mechanism involves a degree of elastic relaxation, such that stress (and strain) gradients will exist across the matrix/inclusion interface (figure 1(a)). In this interfacial region the structural parameters and physical properties associated with the phase transition will clearly differ from those of the free crystals. When the grain size is reduced, the volume proportion of elastically relaxed interfaces increases (figure 1(b)), leading to a second limiting case in which the stress (and strain) become uniform across the matrix/inclusion system (figure 1(c)). Such a uniform material will exist only when the crystallites are at a nanoscale. It might persist only for a finite time, depending on the rates of plastic deformation or fracture, but it might represent the real behaviour of a nanocrystalline ceramic or rock that is heated or cooled on a laboratory timescale.

The two limiting situations have uniform stress and strain distributions arising from thermal expansion effects, and are amenable to straightforward description using Landau theory. In the specific case of the co-elastic transition in quartz, a complete parametrization of the strain and elastic behaviour for free crystals has been given by Carpenter *et al* (1998). The Landau expansion used for the free energy was

$$\begin{aligned} G = {} & \tfrac{1}{2}a(T - T_c)Q^2 + \tfrac{1}{4}bQ^4 + \tfrac{1}{6}cQ^6 \\ & + \tfrac{1}{8}dQ^8 + \lambda_1(e_1 + e_2)Q^2 + \lambda_3 e_3 Q^2 + \lambda_4(e_4^2 + e_5^2)Q^2 \\ & + \lambda_5(e_1e_4 - e_2e_4 + e_5e_6)Q + \lambda_6[e_6^2 + (e_1 - e_2)^2]Q^2 \\ & + \lambda_7(e_1 + e_2)Q^4 + \lambda_8 e_3 Q^4 + \lambda_9(e_1e_4 - e_2e_4 + e_5e_6)Q^3 \\ & + \tfrac{1}{4}(C_{11}^0 + C_{12}^0)(e_1 + e_2)^2 + \tfrac{1}{4}(C_{11}^0 - C_{12}^0)(e_1 - e_2)^2 \\ & + C_{13}^0(e_1 + e_2)e_3 + \tfrac{1}{2}C_{33}^0 e_3^2 + \tfrac{1}{2}C_{44}^0(e_4^2 + e_5^2) + \tfrac{1}{2}C_{66}^0 e_6^2, \end{aligned} \tag{1}$$

where Q is the order parameter (note that Q used in Landau equations is a different parameter to the Q used to represent the quality factor for RUS peak analysis), T_c is the transition temperature, λ_i are strain/order parameter coupling coefficients, e_i are strains and C_{ik}^0 are bare elastic constants (those of β-quartz). The transition is first order in character, occurring at T_{tr}, where

$$(T_{tr} - T_c) = \frac{3(b^*)^2}{16ac^*}. \tag{2}$$

Table 1. Landau parameters taken from the calibration of Carpenter *et al* (1998). For the Pertsev and Salje limit, these were kept the same, except for b^* which was replaced by 0.0396 GPa. $B_{11} = B_{33} = 0.004\,67$ GPa; $B_{12} = B_{13} = -0.001\,09$ GPa.

a	0.000 4135 GPa K^{-1}
b	0.1955 GPa
b^*	−0.081 GPa
c^*	0.430 GPa
T_c	840 K
λ_1	3.38 GPa
λ_3	2.97 GPa
K_0	77.4 GPa

Here b^* and c^* are the renormalized coefficients in

$$G = \tfrac{1}{2}a(T - T_c)Q^2 + \tfrac{1}{4}b^*Q^4 + \tfrac{1}{6}c^*Q^6. \quad (3)$$

This treatment includes higher order strain/order parameter coupling terms which represent a level of detail beyond what is needed here, so terms with coefficients λ_7, λ_8 and the term in Q^8 will not be considered further.

Following Pertsev and Salje (2000), only strains which are non-zero in α-quartz (e_i, $i = 1$–3) are considered to influence the phase transition and (1) can be reduced to

$$G = \tfrac{1}{2}a(T - T_c)Q^2 + \tfrac{1}{4}bQ^4 + \tfrac{1}{6}c^*Q^6 + \tfrac{1}{2}\lambda_i e_i Q^2. \quad (4)$$

It is convenient to express this in terms of elastic compliances, s^0_{ik}, as (after (Pertsev and Salje 2000))

$$G = \tfrac{1}{2}a(T - T_c)Q^2 + \tfrac{1}{4}bQ^4 + \tfrac{1}{6}c^*Q^6 - \tfrac{1}{2}s^0_{ik}\lambda_i\lambda_k Q^4. \quad (5)$$

Renormalization of the fourth order coefficient, b, and coupling between the strain and order parameter are then given by

$$b^* = b - 2[\lambda_3^2 s^0_{33} + 2\lambda_1^2(s^0_{11} + s^0_{12}) + 4\lambda_1\lambda_3 s^0_{13}] \quad (6)$$

$$e_1 = e_2 = -[\lambda_3 s^0_{13} + \lambda_1(s^0_{11} + s^0_{12})]Q^2 \quad (7)$$

$$e_3 = -[2\lambda_1 s^0_{13} + \lambda_3 s^0_{33}]Q^2. \quad (8)$$

The influence of stress, σ, is conventionally treated by adding a term $\sigma_i e_i$. Considering only strains e_1, e_2 and e_3, an isotropic stress (pressure) will induce a volume strain, $2e_1 + e_3$, while anisotropic stresses will induce shear strains such as $e_1 - e_3$. These strains scale with Q^2 in the free crystal so that the net effect of the stress is to renormalize T_c, causing a change in the transition temperature.

Pertsev and Salje (2000) considered the case of a system with uniform stress and randomly distributed ellipsoidal grains in textural equilibrium, as represented schematically in figure 1(c) (the 'elastically clamped' system). They showed that spontaneous strains are partly suppressed such that the excess energy due to the phase transition is reduced to

$$G = \tfrac{1}{2}a(T - T_c)Q^2 + \tfrac{1}{4}bQ^4 + \tfrac{1}{6}c^*Q^6 - \tfrac{1}{2}B^0_{ik}\lambda_i\lambda_k Q^4. \quad (9)$$

The renormalized fourth order coefficient becomes

$$b^* = b - 2[\lambda_3^2 B_{33} + 2\lambda_1^2(B_{11} + B_{12}) + 4\lambda_1\lambda_3 B_{13}] \quad (10)$$

and the relationships between strains and the order parameter change to

$$e_1 = e_2 = -[\lambda_3 B_{13} + \lambda_1(B_{11} + B_{12})]Q^2 \quad (11)$$

$$e_3 = -[2\lambda_1 B_{13} + \lambda_3 B_{33}]Q^2. \quad (12)$$

Here B_{ik} refer to effective elastic compliances for the isotropic inclusion/matrix system, again with values for the reference state, β-quartz. They are given explicitly by Pertsev and Salje as

$$B_{11} = B_{33} = \frac{7 - 10\nu}{30G(1 - \nu)} \quad (13)$$

$$B_{12} = B_{13} = -\frac{1}{30G(1 - \nu)}, \quad (14)$$

where G is the shear modulus, K is the bulk modulus, and $\nu = (3K - 2G)/(6K + 2G)$ is Poisson's ratio.

As values for all the coefficients and the bare elastic constants of β-quartz are known, it is possible to test which of these limiting cases provides a better representation of the real behaviour of nanocrystalline quartz by comparing predicted and observed variations of bulk modulus through the phase transition. The bulk modulus is obtained most simply from single crystal moduli by using the expression for the Voigt limit in the case of hexagonal (622) and trigonal (32) systems (Watt and Peselnick 1980):

$$K = \tfrac{1}{9}[2(C_{11} + C_{12}) + C_{33} + 4C_{13}]. \quad (15)$$

(Note that Voigt values are close to the Reuss values for K, and should therefore provide an adequate representation of the true bulk modulus.) Variations of the individual elastic constants of α-quartz are obtained by applying

$$C_{ik} = \frac{\partial^2 G}{\partial e_i \partial e_k} - \sum_{m,n} \frac{\partial^2 G}{\partial e_i \partial Q_m} \cdot \left(\frac{\partial^2 G}{\partial Q_m \partial Q_n}\right)^{-1} \cdot \frac{\partial^2 G}{\partial e_k \partial Q_n} \quad (16)$$

in the usual way (Slonczewski and Thomas 1970), as listed in table 1 of Carpenter *et al* (1998) for free crystals of quartz.

Pertsev and Salje (2000) pointed out that the treatment of a crystallite inclusion by the 'equivalent inclusion technique' of Eshelby (1957) leads to an expression for a co-elastic transition in which b^* is renormalized to a lesser extent by strain/order parameter coupling than it is in a free crystal (the difference between (6) and (10)). This is because the effective coupling between spontaneous strain and the order parameter is reduced (the difference between (7), (8) and (11), (12)). Their calculations showed that b^* is expected to become positive, so that the evolution of the order parameter becomes the solution to a 246 potential

$$Q^2 = \frac{a}{2c^*}\left(-\frac{b^*}{a} + \sqrt{\left(\frac{b^*}{a}\right)^2 - 4\frac{c^*}{a}(T - T_c)}\right), \quad (17)$$

and the inverse susceptibility, χ^{-1}, becomes

$$\chi^{-1} = \frac{\partial^2 G}{\partial Q^2} = a(T - T_c) + (2b + b^*)Q^2 + 5c^*Q^4. \quad (18)$$

Voigt values of the bulk modulus of α-quartz in the clamped limit are given by

$$K = K^0 - \tfrac{1}{9}(2\lambda_1 + \lambda_3)^2 Q^2 \chi. \qquad (19)$$

Values of the relevant parameters from Carpenter *et al* (1998) are listed in table 1. Variations of e_1 and e_3 for the Pertsev and Salje limit are compared with observed variations of free crystals (Carpenter *et al* 1998) and of quartz in agate samples in figures 2(a) and (b) (data from the study by (Ríos *et al* 2001). Voigt values of the bulk modulus of α-quartz in the Pertsev and Salje limit are compared with variations of the bulk modulus from single crystal elastic constant data of Ohno *et al* (2006) and from the Landau description of Carpenter *et al* (1998) in figure 2(c). There clearly should be marked differences in the properties of free and elastically clamped crystals. In particular, (i) the transition in the clamped system is second order, occurring at $T_c = 567\,^\circ$C instead of first order at $573/4\,^\circ$C, as in free crystals, (ii) spontaneous strains are substantially suppressed in the clamped system and (iii) softening of the bulk modulus is substantially less for the clamped system than for free crystals.

This full limiting behaviour applies strictly only to nanocrystalline ceramics with grain boundaries equilibrated in the stability field of the reference phase, β-quartz. Natural polycrystalline samples have grain boundary equilibration temperatures which are probably within a few hundred degrees of room temperature. In this range, values of their spontaneous strains and elastic moduli might match the average values from single crystal data since their grain boundaries will be more or less stress free. A tendency towards nanolimits is then expected to occur as stresses due to anisotropic thermal expansion build up with increasing temperature.

These Landau descriptions of the behaviour of α-quartz do not provide information on the elastic softening in β-quartz ahead of the transition. Values of K for β-quartz shown in figure 2(b) were obtained by fitting an empirical function to single crystal data, and using the Voigt/Reuss/Hill average (Carpenter *et al* 1998, Carpenter 2006).

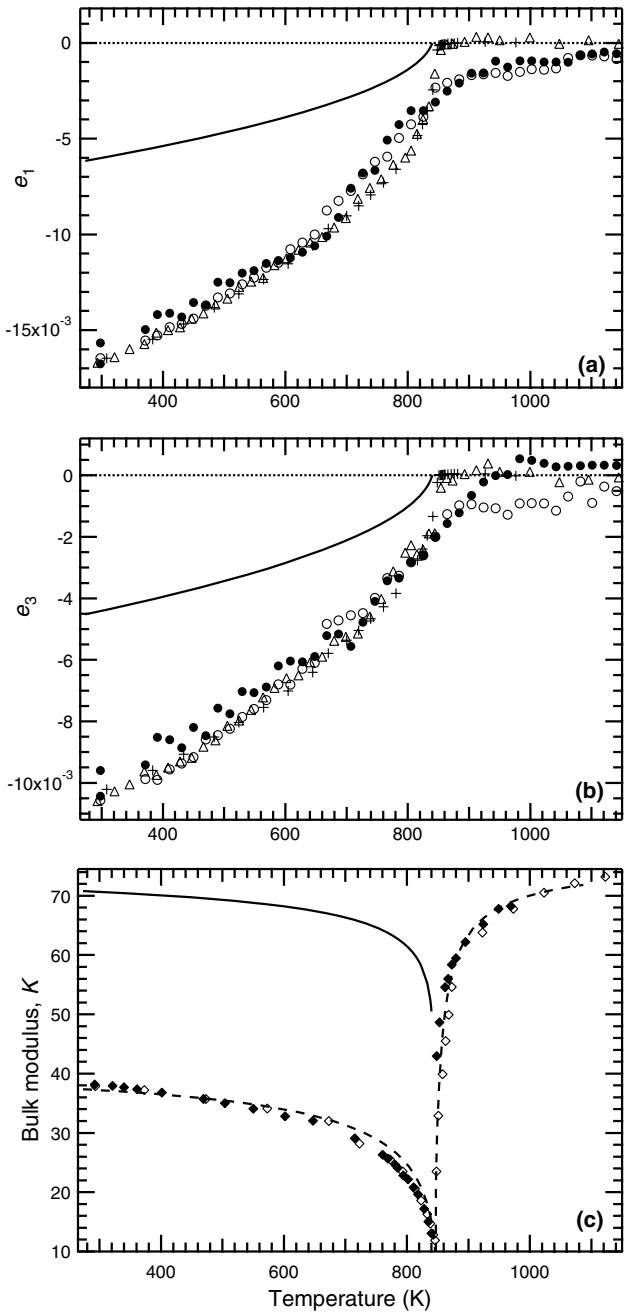

Figure 2. Comparison of observed strain and bulk modulus variations with predictions based on the Pertsev and Salje (2000) model for nanocrystalline quartz. Spontaneous strains in (a) and (b): crosses and triangles are neutron diffraction and x-ray diffraction data respectively, from a crushed sample of single crystal quartz (Carpenter *et al* 1998). Open and closed circles are strains calculated using the lattice parameter data of two agate samples (from Iran and Ardownie respectively), with reported grain sizes of ∼90 nm from Ríos *et al* (2001); in calculating strains from these data, reference parameters for β-quartz of Carpenter *et al* (1998) were used. Solid lines are strains calculated using equations (11) and (12), with values of the relevant parameters given in table 1. (c) The solid line represents values of K calculated using equation (19). Broken lines are values calculated using a Landau parametrization of the phase transition (Carpenter *et al* 1998, Carpenter 2006, Carpenter *et al* 2006). Filled diamonds and open diamonds are Voigt/Reuss/Hill averages of single crystal data from Ohno *et al* (2006) and Lakshtanov *et al* (2007), respectively.

3. Experimental details

3.1. Apparatus

The high temperature RUS setup used for the experiments described here consists of two alumina rods, mounted horizontally. Piezoelectric transducers are attached to one end of each rod and the sample is balanced across its corners between the other ends (figure 3), in an arrangement that is similar to the design described by Schreuer and Haussühl (2005) and Schreuer *et al* (2006). One transducer acts as the driving resonator and the other as the detector for ultrasonic frequencies, using dynamic resonance system (DRS) M^{3}odulus II electronics. A Netzsch 1600 °C furnace is slid over the rods for high temperature measurements. The temperature is determined during heating and cooling cycles using a thermocouple placed a few millimetres away from the sample. The estimated precision and stability for quoted sample temperatures is ±0.3 °C.

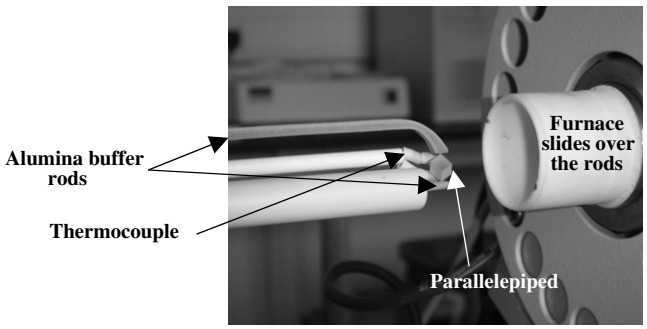

Figure 3. The high temperature RUS setup, showing a parallelepiped balanced on its opposite corners between two horizontal alumina rods, which are connected at the other end to piezoelectric transducers. For scale, each edge of the parallelepiped is ∼5 mm.

Measurements were also obtained from the novaculite sample using a low temperature RUS setup. Again, the standard RUS arrangement controlled by a DRS M^3odulus II system is used. In this case, the parallelepiped is mounted directly onto the piezoelectric transducers in a RUS head made mainly from Tufnol composite G10/40 to reduce mechanical linkages between the transducers other than through the sample (McKnight *et al* 2007). The bottom piezoelectric transducer is shielded with copper or gold foil to reduce radio frequency interference. The whole RUS head is mounted on the end of a stick and lowered into a standard Orange 50 mm helium flow cryostat, supplied by AS Scientific Products Ltd. Temperature regulation and measurement is achieved using a silicon diode and a LakeShore model 340 controller. All materials for elements used in the system, including the wires connecting the RUS head to exit points from the cryostat, were specially selected so that they operated well down to temperatures as low as ∼5 K. Data can be collected during cooling and heating cycles in a temperature range of ∼5–300 K with the temperature stability for each measurement being approximately ±0.1 °C. Sequences of data collection (temperature range, temperature intervals, rest time at each temperature) are controlled using software developed in-house to drive the furnace or cryostat and the DRS electronics.

3.2. Sample description

The samples used for this study were all natural polycrystalline silica (SiO_2) minerals with varying grain sizes. Table 2 summarizes the relevant properties of each sample at room temperature before and after the experiments were carried out.

Three agate samples all showed typical colour banding implying some degree of anisotropy. The Brazilian agate, purchased from a mineral dealer and originally collected from the Soledade mines in Rio Grande do Sul, Brazil, was mainly light grey/translucent, with a few reddish areas. Colour banding was not obvious but was clearly evident when a translucent slice was held up to the light. The parallelepiped used for the experiment was cut from one of the completely light-coloured areas, avoiding the red areas. The Mexican agate sample, collected from Ojo Laguna, Chihuahua, Mexico, was a deep orange/pink colour with some small (<1 mm) areas of dark red. The parallelepiped was cut so as to try and avoid the dark red areas. Agate from Ethiebeaton in Scotland was a nodule approximately 5 cm in diameter, showing wall-lining banding with a gradual colour gradation from near-black bands on the edge of the sample through to brown, finishing with a grey translucency in the centre. The parallelepipeds used for this experiment were cut from a translucent area close to the centre of the specimen. A white/grey novaculite from Arkansas, USA, was composed of 99.898% pure silica and only trace amounts of other elements (0.02% Al, 0.0005% B, 0.03% Ca, 0.05% Mg, 0.0007% Mn). The sample (and associated chemical information given here) was obtained from Dan's Whetstone Company and was mined from the quarry named Dan's Pit #1 in the translucent site. The quartzite sample was one from the general teaching collection at the University of Leeds and originally came from Banff in Scotland. It was pinkish/grey in colour, probably due to the presence of a small amount of iron oxide (<1%). A granular texture was visible to the naked eye.

Crystallite sizes of the agates were calculated using powder x-ray diffraction data. Powders were crushed and ball-mill ground to <10 μm. The powders used were ground-up offcuts from the same area of each sample that was used to cut the parallelepipeds from. The preparation process of the <10 μm powders used for this procedure has been described elsewhere (Moxon 2002). XRD runs were carried out using a Bruker D8 diffractometer with Cu Kα radiation in reflection mode. The crystalline phases were found over the 16°–52° 2θ range using a step size of 0.02°. Separate runs were used to calculate the crystallite size from the (101) quartz reflection at 26.64° 2θ with a scan over 16°–30° 2θ range and a step size of 0.01°. Corrections for instrument broadening were made with added Si (28.44° 2θ) as an internal standard. The crystallite size (C_s (101)) was calculated using the Warren correction within the Scherrer equation. Each agate sample was run twice in the diffractometer and a mean grain size value from both runs is given in table 2. The grain size of quartzite was estimated from the examination of a thin section under a standard petrographic microscope. The crystallite size of Arkansas novaculite has previously been reported as 1–5 μm from scanning electron microscopy observations (Keller *et al* 1977, 1985).

The only crystalline phase in Ethiebeaton agate and novaculite, identified from x-ray diffraction data, was α-quartz. However, the silica polymorph, moganite (Heaney and Post 1992), was found to occur in both Mexican and Brazilian agates, in addition to α-quartz. The overlap of the moganite and quartz peaks gives a poor sensitivity when determining low levels of moganite using Rietveld refinement. An alternative estimation of the moganite content was discussed by Moxon and Ríos (2004). Here, the strongest moganite peaks at ∼20° 2θ and the (100) quartz peak are employed. A scan over 17°–23° 2θ with a 0.02° step size for 20 s are used. This 2θ range is given a constant background and fitted with two Lorentzian functions. The moganite content is estimated from the ratio: peak area of moganite/total peak area. Using this method, the estimated error is ±2% and the determined moganite contents in the Mexican and Brazilian agates are 11% and 21% respectively. These are given in table 2.

Table 2. Properties of samples at room temperature before and after the experiments were carried out; compared to single crystal properties from resonant ultrasound spectroscopy and Brillouin spectroscopy.

Sample	Single crystal quartz (using the RPR method)[a]	Single crystal quartz (using Brillouin spectroscopy)[b]	Brazilian agate	Mexican agate	Ethiebeaton agate	Novaculite	Quartzite
Sample number			BR64 1	MEX7a 3	EQ12 1	NOVC1	BQ8585 2
Origin	Synthetic	Brazil	Soledade mines, Rio Grande Do Sul, Brazil	Ojo Laguna, Chihuahua, Mexico	Ethiebeaton Quarry, Tayside, Scotland	Ouichita Mountains, Arkansas, USA	Banff, Scotland
Colour			Grey/translucent	Orange/pink	Translucent	White/grey	Pink/translucent
Weight (g)	0.039 87		0.2359	0.1858	0.1736	0.1588	0.1575
	1.622	∼1	3.688	3.410	3.499	2.866	3.002
Dimensions (mm)	2.915	∼2	4.699	3.926	3.787	4.437	4.002
	3.193	0.075–0.15	5.333	5.408	4.999	4.798	5.000
Density (g cm^{-3})	2.641	2.649	2.552	2.566	2.621	2.603	2.622
Estimated porosity (%)			3.4	2.8	0.8	1.4	0.7
Grain size	Single crystal	Single crystal	49.8 nm ± 5%	64.4 nm ±5%	121.1 nm ± 5%	1–5 μm[c]	0.1–0.3 mm
Total water content (%)			1.22	1.24	0.28	0.11	
Free water content (%)			0.21	0.43	0.05	0.05	
Moganite content (%)	0	0	21	11	0	0	0
Bulk modulus, K (GPa)	38.17	37.9	34.84	33.9	34.3	36.9	39.9
Shear modulus, G (GPa)	44.86	44.9	46.6	36.98	44.28	43.33	37.01
RMS error for fit (%)			2.31	0.35	1.12	0.24	2.74
Estimated transition temperature (°C)	573/574.3 (α/β)	573	575[d]	Smeared	573[d]	580[d]	573
			After heating				
Colour			Opaque milky white core with translucent edge	Deep orange/red	Opaque milky white throughout	No colour change	Pink/white
Weight (g)				0.1841	0.1732	0.1586	0.1572
Dimensions (mm)			Broke apart at 795–800 °C	3.409 3.920 5.404	3.519 3.814 5.032	2.862 4.431 4.789	3.003 4.004 5.003
Density (g cm^{-3})				2.549	2.565	2.611	2.613

[a] Ohno *et al* (2006).
[b] Lakshtanov *et al* (2007).
[c] Keller *et al* (1977, 1985).
[d] Transition temperatures quoted here include calibration of the thermocouple readings against the transition temperature of single crystal quartz (573 °C).

Parallelepipeds were cut from all the mineral specimens using a fine annular diamond saw, lubricated with paraffin. During the cutting process, samples were glued to glass blocks using Crystalbond glue, manufactured by SPI supplies, with a softening temperature of 120–130 °C. A parallelepiped of single crystal quartz was also cut from a large crystal, with edges oriented along the [001], [100] and [120] directions.

The agate samples were crushed and sieved to <52 μm in order to calculate their water contents. Free molecular water was determined from the difference in mass before and after heating fresh powder in a box oven at 170 °C for 4 h. Total water content (silanol and free water) was determined by furnace heating fresh powders at 1200 °C for 2 h. These heating times were sufficient to produce a constant mass loss. Each run was carried out in triplicate. Previous studies have investigated agate dehydration over the 20–1400 °C temperature range ((Moxon and Ríos 2004), and references therein). Thermogravimetric analysis plots show that loosely bound water is completely lost at ∼120 °C, with minimal further water loss to 200 °C. Heating at higher temperatures removes tightly bound water and silanol water (SiOH) resulting in complete dehydration at 1000 °C. Free and total water contents calculated from the dehydration investigation of novaculite, Ethiebeaton, Mexican and Brazilian agates are shown in table 2.

3.3. Data collection and analysis

Room temperature RUS spectra were measured for all samples in the frequency range 100–2000 kHz with the sample in four different orientations to ensure that all resonances in the spectra were excited and observed. Spectra collected at high temperatures each contained 50 000 data points over frequency ranges between 200 and 1200 kHz. All the spectra were transferred to the software package Igor Pro (WaveMetrics) for detailed analysis. Peak positions and halfwidths were determined for selected peaks by fitting with an asymmetric Lorentzian function, an approach analogous to that described by Schreuer *et al* (2003) and Schreuer and Thybaut (2005). The mechanical quality factor, Q, is given by $Q = f/\Delta f$, where f is the peak frequency and Δf is the peak width at the half-maximum point.

Bulk and shear moduli (K and G respectively) were determined by matching observed peak frequencies with

calculated frequencies for 10–25 resonance peaks using the DRS software (Migliori and Sarrao 1997) and assuming an isotropic medium. Starting values for this fitting process were the Hill averages for bulk and shear moduli of single crystal quartz calculated by Ohno *et al* (2006). Percentage RMS errors for the room temperature fits are given in table 2. This RMS error describes the quality of fit between calculated and observed resonance frequencies. Following Migliori and Sarrao (1997), an RMS error of 0.1–0.2% is considered to imply a 'good' fit. Relatively poor fits, i.e. above ∼2%, are interpreted here as being due to anisotropicity. Uncertainties in the extracted values of K and G, respectively, are 1.8 and 0.98 GPa for quartzite (RMS error 2.74%); 0.12 and 0.10 GPa for novaculite (RMS error 0.14%); 0.54 and 0.50 GPa for Ethiebeaton agate (RMS error 1.12%); 0.20 and 0.15 GPa for Mexican agate (RMS error 0.35%); and 1.8 and 0.77 GPa for Brazilian agate (RMS error 2.31%). These uncertainties are estimated by measuring the changes in independent parameters when the chi-squared 'goodness of fit' value is increased by 2%.

The Brazilian agate and quartzite both show large RMS errors (>2%), suggesting they are somewhat anisotropic. Novaculite and Mexican agate both gave relatively good fits (RMS errors <1%). In every spectrum the lowest frequency resonance peak depends only on the shear modulus, while all other peaks depend on some mixture of K and G. Room temperature values of K and G are given in table 2 alongside Voigt/Reuss/Hill averages from RUS (Ohno *et al* 2006) and Brillouin spectroscopy (Lakshtanov *et al* 2007).

Changes in parallelepiped dimensions and density due to thermal expansion only have a small effect on computed values of K and G. Their room temperature dimensions were therefore used for fitting of all the high temperature spectra.

The estimated transition temperatures quoted in table 2 were the temperatures at which each sample showed a minimum in the variation of peak frequency with temperature. The parallelepiped of single crystal quartz was used to provide an independent calibration of temperature in the vicinity of the α–β transition point.

3.3.1. Quartzite. High temperature measurements were taken for quartzite during heating from room temperature up to 765 °C, with intervals of 10, 5, 1 °C between measurements. The smaller temperature increments were used in the vicinity of the α–β phase transition. The sample was then cooled from 775 °C to room temperature in 20 °C intervals. The settle time at each temperature was 15 min.

3.3.2. Novaculite. RUS spectra for novaculite were collected at temperatures between −253 and 840 °C. The sample was initially cooled from room temperature to −253 °C, with data collection every 20 °C and a 30 min settle time at each step. The sample was then heated back to room temperature in 5 °C steps with 15 min settle times. The sample was then transferred to the high temperature RUS system and heated up to 839 °C. Spectra were collected at intervals of 10, 5 and 1 °C, with the smaller temperature increments in the vicinity of the α–β phase transition. Finally, the sample was cooled back to room temperature with data collection every 30 °C and a 15 min settle time at each step. A second sample was heated in a similar way with 1 °C intervals in the vicinity of the transition to pinpoint the exact transition temperature.

3.3.3. Ethiebeaton agate. Ethiebeaton agate was heated from room temperature to 500 °C in 10 °C intervals and then from 505 to 840 °C in 5 °C intervals. The settle time at each temperature was 15 min. No spectra were collected during cooling back to room temperature due to a problem with the computer software. The same sample was heated from room temperature back up to 516 °C in 10 °C intervals in order to assess how the sample may have been affected by heating through the phase transition. A second sample was heated in a similar way with 1 °C intervals in the vicinity of the transition to pinpoint the transition temperature.

3.3.4. Mexican agate. The agate from Mexico was heated from room temperature up to 784 °C with intervals of 10, 5, 1 °C between measurements. The smaller temperature increments were used in the vicinity of the α–β phase transition. The sample was then cooled from 763 °C back to room temperature collecting spectra every 10 °C with a 15 min settle time at each step, except within ∼25 °C either side of the transition point when the intervals between measurements were 1 °C with a 10 min settle time.

3.3.5. Brazilian agate. Spectra were collected every 10 °C from room temperature up to 500 °C, and then in 5 °C intervals up to 795 °C. The settle time at each step was 15 min. The sample broke into two pieces and a number of small fragments before the next spectrum was measured at 801 °C.

4. Results

4.1. Quartzite

Figure 4(a) shows a stack of spectra collected for quartzite during heating and figure 5(a) shows the evolution of individual resonance peaks. All resonances show a decrease in frequency from room temperature up to the phase transition, with a more pronounced curvature in the temperature evolution as the phase transition is approached (figure 4(b)). This is directly comparable to single crystal behaviour seen in the study by Ohno *et al* (2006). A minimum in the resonant frequencies occurs in the spectrum collected at 573.6 °C (figure 5(a)). This is indistinguishable from the known transition temperature of natural quartz, 573/574 °C, (Raz *et al* 2003). Above this point, however, the resonances do not recover as much as would be expected based on the known elastic properties of quartz. There is only a very slight recovery of the frequencies up to ∼590 °C, when they become approximately constant up to the highest temperature reached, 765 °C (figure 5(a)). The evolution on subsequent cooling was quite different from the heating sequence (figure 4(c)), showing that some irreversible changes had occurred in the sample.

Features that are common to all resonance peaks are the low Q and high Q^{-1} from room temperature up to ∼200 °C,

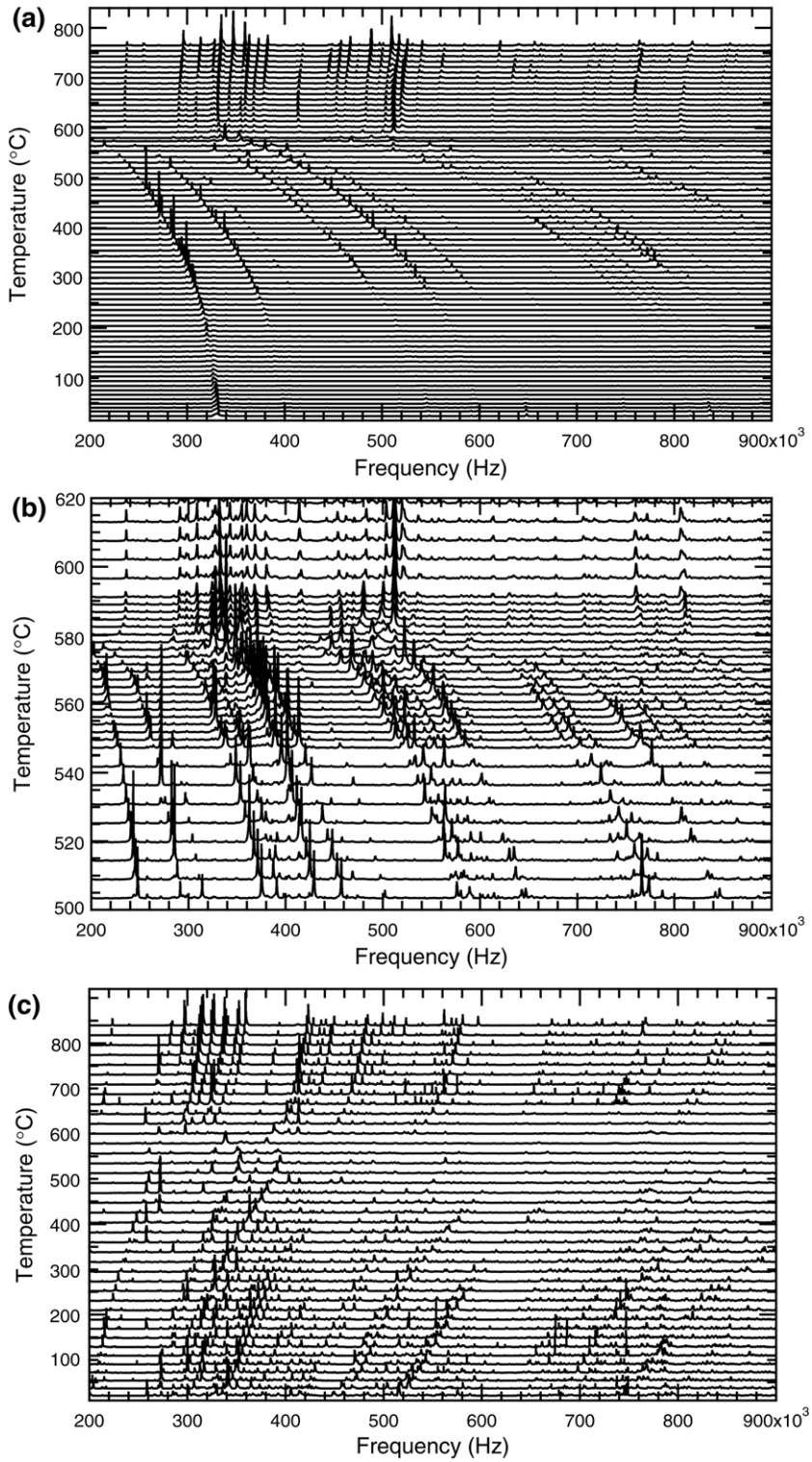

Figure 4. RUS spectra for polycrystalline quartzite BQ8585 in the frequency region 200–900 kHz, (a) at intervals during heating from room temperature up to 765 °C; (b) at intervals in the region from 500 to 620 °C during heating; and (c) during cooling from 775 °C down to room temperature. In this and subsequent spectra plots, the **y**-axis is amplitude but the spectra have been displaced in proportion to the temperature at which they were collected. This temperature scale is then shown as the **y**-axis.

followed by a sudden decrease in dissipation across about a 50 °C range, and then a large peak in dissipation (minimum Q, maximum Q^{-1}) at the transition point (figures 5(b) and (c)).

4.2. Novaculite

Figure 6(a) shows a stack of spectra collected for novaculite during heating from −253 °C up to 839 °C and figure 7(a) shows the evolution of individual resonance peaks. The

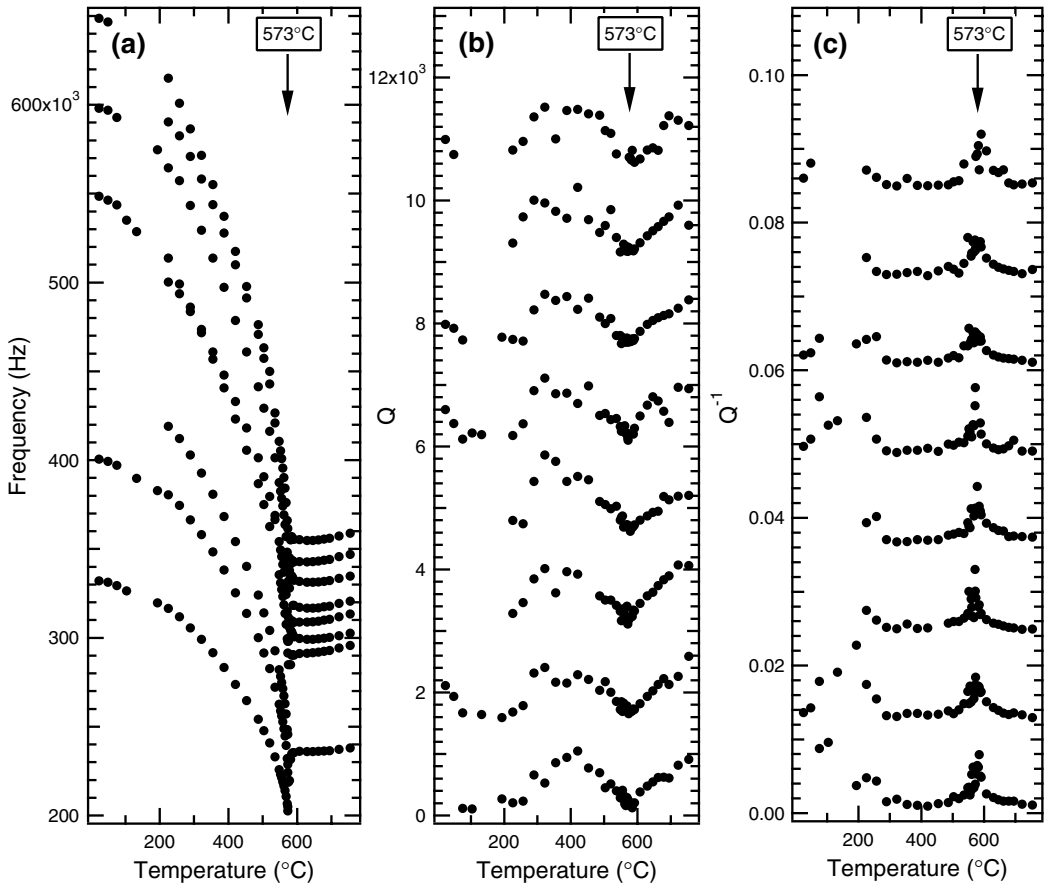

Figure 5. (a) Frequency variation; (b) quality factor (Q) variation; and (c) inverse quality factor (Q^{-1}) variation for the first 8 measurable peaks in the spectra shown in figure 3(a), for quartzite BQ8585, collected during heating from room temperature up to 765 °C. Values of Q and Q^{-1} for each peak are offset from zero by different amounts for ease of inspection. The expected α–β transition temperature, 573 °C, is marked in each figure with an arrow.

pattern observed is very similar to that seen for individual single crystal elastic constants (Ohno *et al* 2006). Resonant frequencies decrease very slightly from −253 to ∼400 °C and then with a much steeper slope as the transition is approached from below. Most peaks disappeared in the vicinity of the transition point but those which can be followed show a clear minimum in frequency in the spectrum collected at 583 °C. Their frequencies increase steeply above the phase transition before levelling off above ∼665 °C. For some resonances there is a softening and subsequent recovery, due to the phase transition, of up to 100 kHz in the temperature region 400–665 °C. The pattern of evolution of spectra during cooling (figure 6(b)) is the same as observed during heating.

All resonances analysed show an increase in Q below ∼−100 °C and a small but noticeable maximum in Q at ∼350 °C (figure 7(b)). The peak in dissipation at the phase transition is similar to that seen for quartzite (figure 7(c)). The behaviour below −100 °C is shown more clearly as a broad peak in dissipation at ∼ − 50 °C (figure 7(d)).

4.3. Ethiebeaton agate

Figure 8(a) shows a stack of spectra collected for Ethiebeaton agate during heating from 29 °C up to 840 °C and figure 8(b) shows the evolution of individual resonance peaks. The pattern observed in figure 8(b) is again similar to that seen for individual single crystal elastic constants (Ohno *et al* 2006). Resonant frequencies decrease by up to 150 kHz and a minimum occurs at 576 °C (figure 8(b)). Resonances did not disappear in the vicinity of the phase transition to the same extent that they did for novaculite. Above the phase transition, the pattern of evolution is of recovery up to ∼670 °C followed by a decline in frequency. Comparison of the room temperature spectra before and after the experiment shows that the sample had been affected by the heat treatment to some extent, as the resonances were observed at different frequencies. The same number of resonances were still present with the same distribution, however, suggesting that it remained a single coherent parallelepiped. A second heating run of the sample showed the same pattern of frequency evolution as obtained in the first run (figure 8(b)) with all peaks occurring at frequencies reduced by ∼8% compared to the values obtained from the first heating run.

Figures 8(c) and (d) show the evolution of Q and Q^{-1} respectively for 8 resonance peaks. There are 3 peaks in dissipation which appear to be common to all resonances: one at ∼100 °C, one at ∼200 °C, and one at the transition temperature. There is also a peak in Q between 350 and 400 °C.

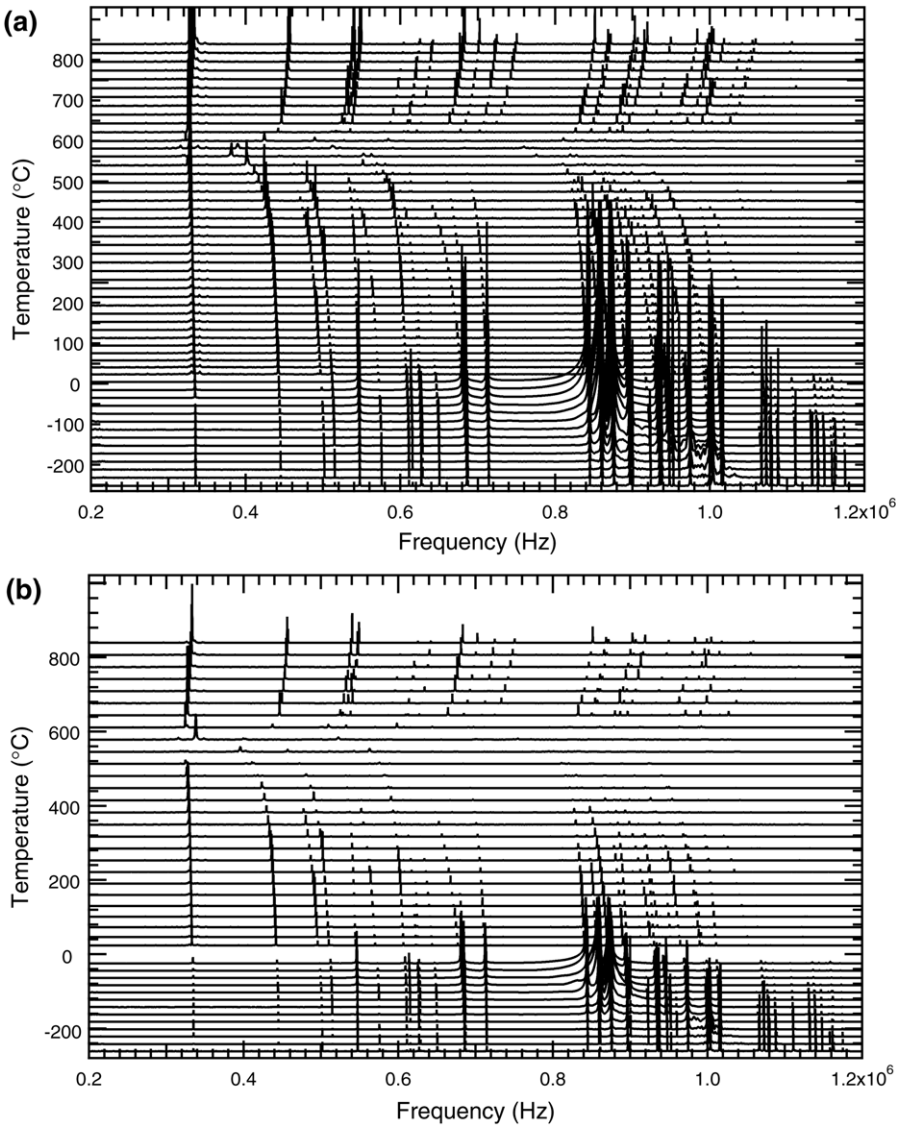

Figure 6. RUS spectra measured at regular intervals in the frequency region 200–1200 kHz during (a) heating from −253 °C up to 839 °C; and (b) cooling from 840 °C down to −263 °C, for novaculite NOVC1. The spectra below room temperature were measured with the sample in the cryostat; those above room temperature were measured with the sample in the furnace.

Other anomalies in Q and Q^{-1} are visible; however they are not common to all resonances and can mostly be attributed to overlapping peaks in the spectra.

4.4. Mexican agate

Figures 9(a)–(d) show the stacked spectra, frequency evolution, Q and Q^{-1} respectively for the Mexican agate during heating from 23 °C up to 784 °C. There is a slight dip in frequencies at approximately 150 °C and then a much larger softening that is clearly a result of the phase transition (figure 9(b)). Frequencies of all the resonance peaks recover in the stability field of β-quartz. Note that in this case, the softening is much less pronounced than was found for quartzite, novaculite and Ethiebeaton agate. The transition temperature was also more difficult to specify as the minima in frequencies were spread out over several degrees.

Q and Q^{-1} for the six peaks examined in detail all indicate a large decrease in dissipation from room temperature up to ∼300 °C, followed by a very slight increase as the transition point is approached. There is then a peak in Q^{-1} clearly associated with the phase transition.

Spectra obtained during heating and cooling were closely similar, showing that the sample did not undergo any obvious irreversible changes associated with heating above the transition point.

4.5. Brazilian agate

Figure 10(a) shows the stack of spectra collected for the Brazilian agate during heating from 29 °C up to 795 °C, and figure 10(b) shows the evolution of individual peaks. It was intended to collect data to higher temperatures but the spectrum collected at 801 °C indicated that the parallelepiped

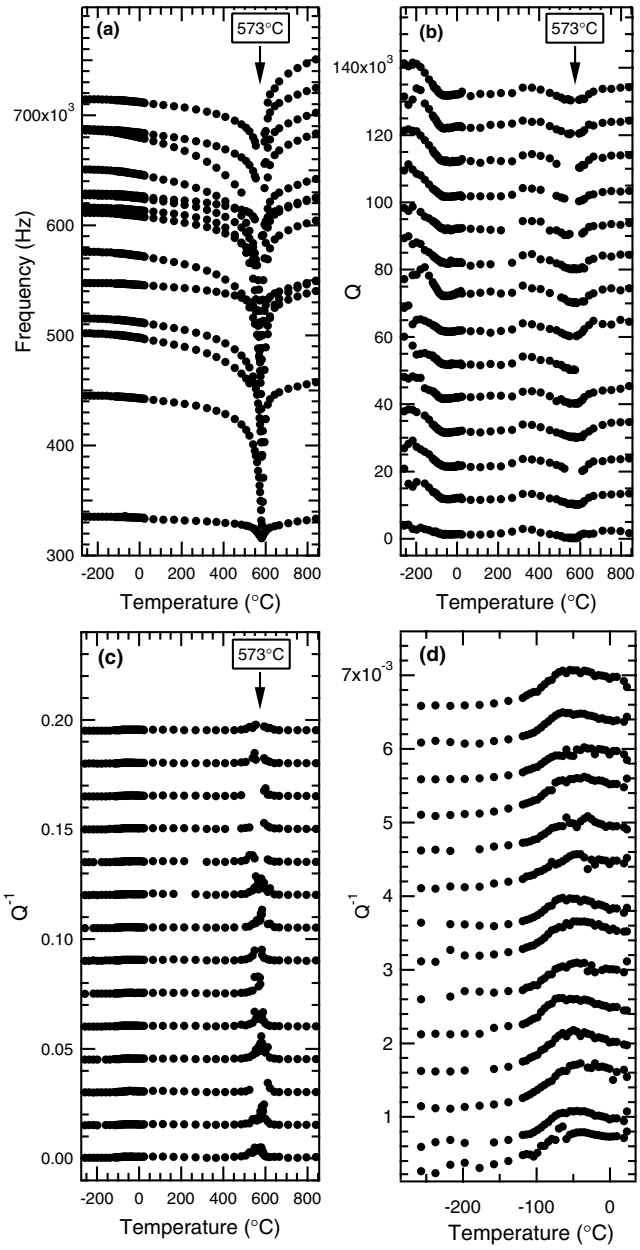

Figure 7. (a) Frequency variation; (b) quality factor (Q) variation; and (c) inverse quality factor (Q^{-1}) variation for the first 14 measurable peaks in the spectra shown in figure 6(a), for novaculite NOVC1, collected during heating from −257 to 839 °C. Values of Q and Q^{-1} for each peak are offset from zero by different amounts for ease of inspection. The expected α–β transition at 573 °C is marked in each figure with an arrow. (d) is an expanded section of (c) showing the evolution of Q^{-1} for novaculite NOVC1 in the temperature region −257 to 10 °C to highlight the small peak at −50 °C.

had fallen off the alumina rods, due to the fact that it had broken into pieces. Resonances decrease in frequency steadily from room temperature to ∼300 °C, where there is a minimum (figure 10(b)). This corresponds to the temperature of the *Imab–I2/a* transition in moganite (Heaney and Post 2001, Heaney *et al* 2007). There is then a slight recovery, with frequencies increasing between approximately 300 and 400 °C, before they start to decrease again towards the quartz phase transition temperature. The maximum amount of softening seen in this sample is the lowest of all samples, with only about 30 kHz change in any resonance. The frequency minima occur at 578 °C, but again the transition point appears to be smeared out. Frequencies recover in the β-phase by a maximum of ∼60 kHz in a similar way to the pattern observed for novaculite, Ethiebeaton agate and Mexican agate. Resonance modes were easy to follow by inspection as they did not disappear in the vicinity of the phase transition.

Q is generally high for this sample ($\gg 100$), except below 200 °C (figure 10(c)). There are three peaks in dissipation common to all modes: one at ∼100 °C, a very small one at ∼300 °C, and a large one at the α–β transition temperature (figure 10(d)). There is a sudden increase in Q^{-1} at ∼780 °C. This may, however, have been due to changes in strain that caused the sample to break, rather than internal dissipation processes.

When the sample was extracted from the furnace, after cooling to room temperature, it was noted that it had shattered across the centre of the parallelepiped. On closer examination, the core (about half of the diameter of the sample) had changed colour to an opaque white, while the outer half remained the translucent light grey colour that the whole sample had been before the experiment.

4.6. Single crystal quartz and calibration of transition temperatures

The RUS experiments were conducted over a period of 10 months and it is possible that some drift in the properties of the thermocouple close to the sample occurred during this time. The quartzite sample, run at an early stage, gave the expected transition temperature of 573 °C. Agate samples were run at a later stage and gave transition temperatures, as indicated by minima in resonance frequencies, of 576 °C (Ethiebeaton) and 578 °C (Brazil). Single crystal quartz consistently gave a transition point of 576/577 °C in repeated RUS runs interspersed with reruns of the novaculite sample, Ethiebeaton agate, and the primary run for the Mexican agate. Novaculite had a transition temperature of 582/583 °C and Ethiebeaton agate had a transition temperature of 576 °C. These results are interpreted as indicating that the thermocouple was giving temperatures ∼3 °C in excess of the true temperature at 573 °C and that the agate samples had transition temperatures close to 573 °C. Novaculite thus has a transition temperature ∼7 °C above that of single crystal quartz and other polycrystalline samples.

4.7. Elastic constant variations

For the quartzite sample, fits between observed and calculated resonance frequencies were poor at room temperature (RMS error = 2.7%). Attempts were made to fit spectra at higher temperatures where peaks were better resolved, but the same problem was encountered. This suggests that this sample is anisotropic. In thin section, individual grains appeared to have uniform size and shape suggesting that the anisotropy is due to some preferred alignment of crystallographic axes rather than to grain texture.

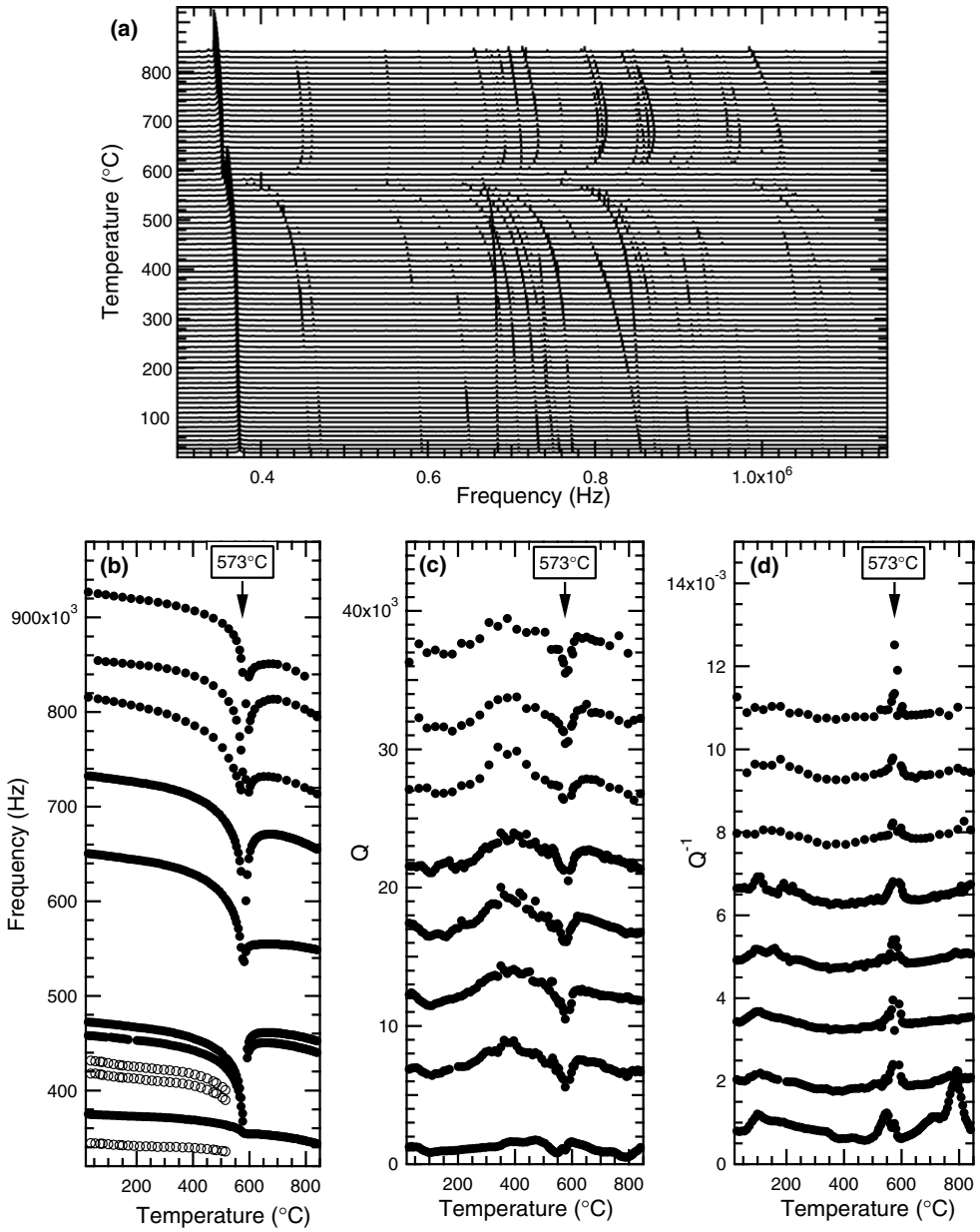

Figure 8. Data for Ethiebeaton agate EQ12 collected at intervals during heating from 29 to 840 °C. (a) shows RUS spectra in the frequency range 300–1150 kHz; (b), (c) and (d) show frequency, quality factor (Q), and inverse quality factor (Q^{-1}) variation respectively (closed circles) for 8 measurable peaks in the spectra shown in (a). Open circles in (b) show the resonances of the same sample heated to 516 °C for a second time. Values of Q and Q^{-1} for each peak are offset from zero by different amounts for ease of inspection. The expected α–β transition at 573 °C is marked in each figure with an arrow.

Peaks in the room temperature spectra for novaculite were well resolved and the fit for elastic constants was very good (RMS error = 0.24%). Absolute values of bulk and shear moduli are comparable to those expected from single crystal data (see table 2). The room temperature values ($K = 36.9$ GPa and $G = 43.33$ GPa) were used as starting values for fits at all other temperatures. The fitted values for K and G, based on 10–25 peak positions, are included in figures 11(a) and (b) respectively. Even in the vicinity of the phase transition, where resolution of peaks deteriorates, the maximum RMS error was still low (∼0.6%). Due to the difficulty of measuring weak peaks, it was not possible to obtain any fits in the temperature region 560–595 °C. Comparison with Voigt/Reuss/Hill averages calculated by Ohno *et al* (2006) and by Lakshtanov *et al* (2007), also plotted on figures 11(a) and (b), show that novaculite values are systematically lower than the Hill averages for single crystal quartz. It can also be noted that there is a small anomaly in both K and G that occurs at −50 °C. This corresponds with the peak in Q^{-1} seen at the same temperature.

The peaks in the room temperature spectra of Ethiebeaton agate were moderately well resolved, the fit for elastic constants was reasonable (RMS error = 1.2%) and elastic constants comparable to those from single crystals were

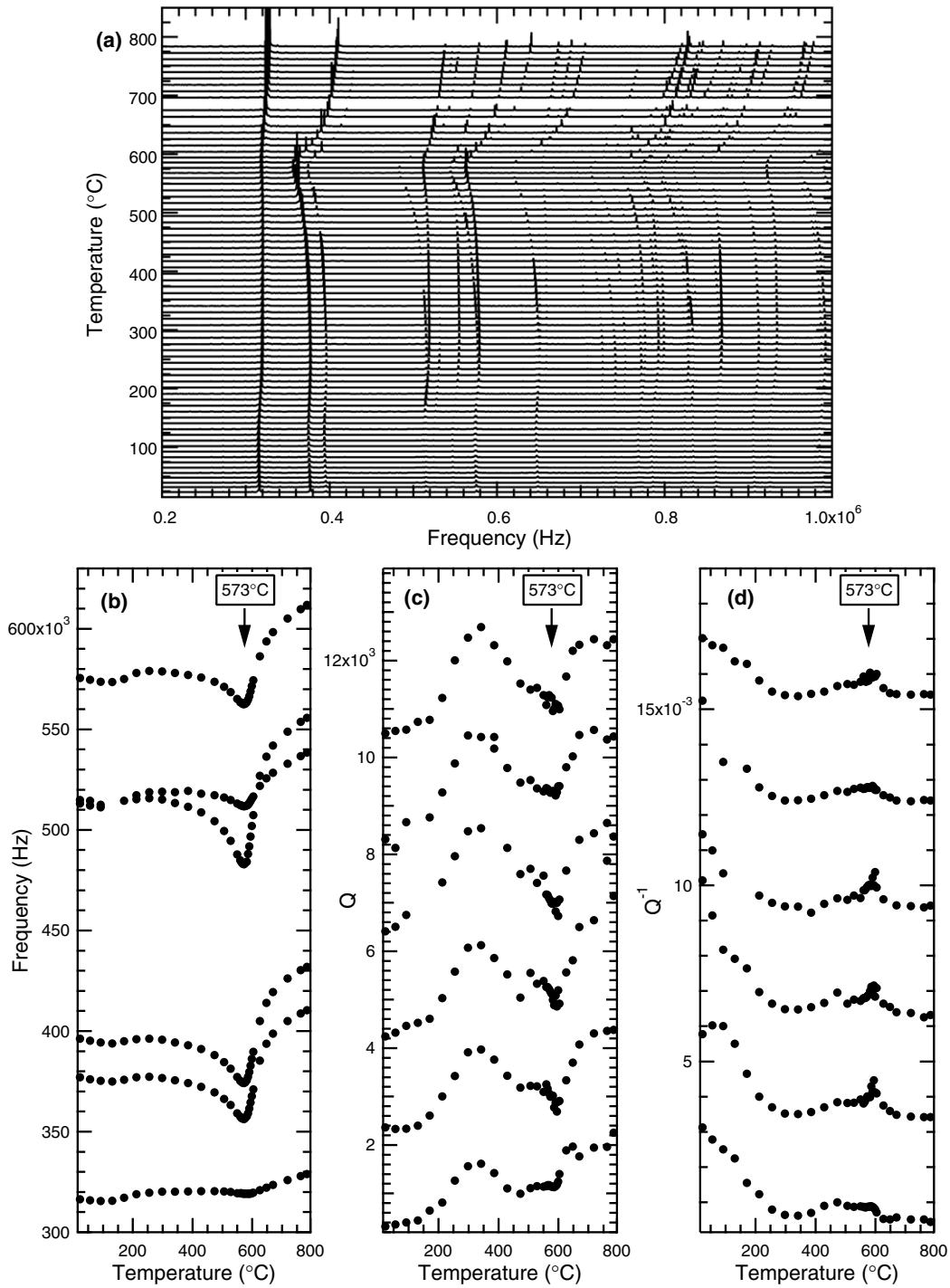

Figure 9. Data for Mexican agate MEX7a collected during heating from 23 to 784 °C. (a) RUS spectra in the frequency range 200–1000 kHz. (b)–(d) Frequency, quality factor (Q), and inverse quality factor (Q^{-1}) variation respectively for 6 measurable peaks in the spectra shown in (a). Values of Q and Q^{-1} for each peak are offset from zero by different amounts for ease of inspection. The expected α–β transition temperature, at 573 °C, is marked in each figure with an arrow.

obtained (see table 2). The values of K (34.3 GPa) and G (44.28 GPa) were used as starting values for fits at all other temperatures. The fitted values for K and G, based on 10–25 peak positions, are included in figures 11(a) and (b) respectively. Refinements were reasonable across the full temperature range (RMS error <2%), except in the temperature region 560–576 °C where there were not enough well-resolved peaks in the spectra to assign individual resonances for a fit. Refinements were better (RMS error <1%) for the data taken for the second sample and these are plotted in figures 11(a) and 11(b) in the vicinity of the transition temperature for completion. The evolution of K and G with temperature follows the same pattern as individual single crystal elastic constants up to ∼680 °C, with elastic

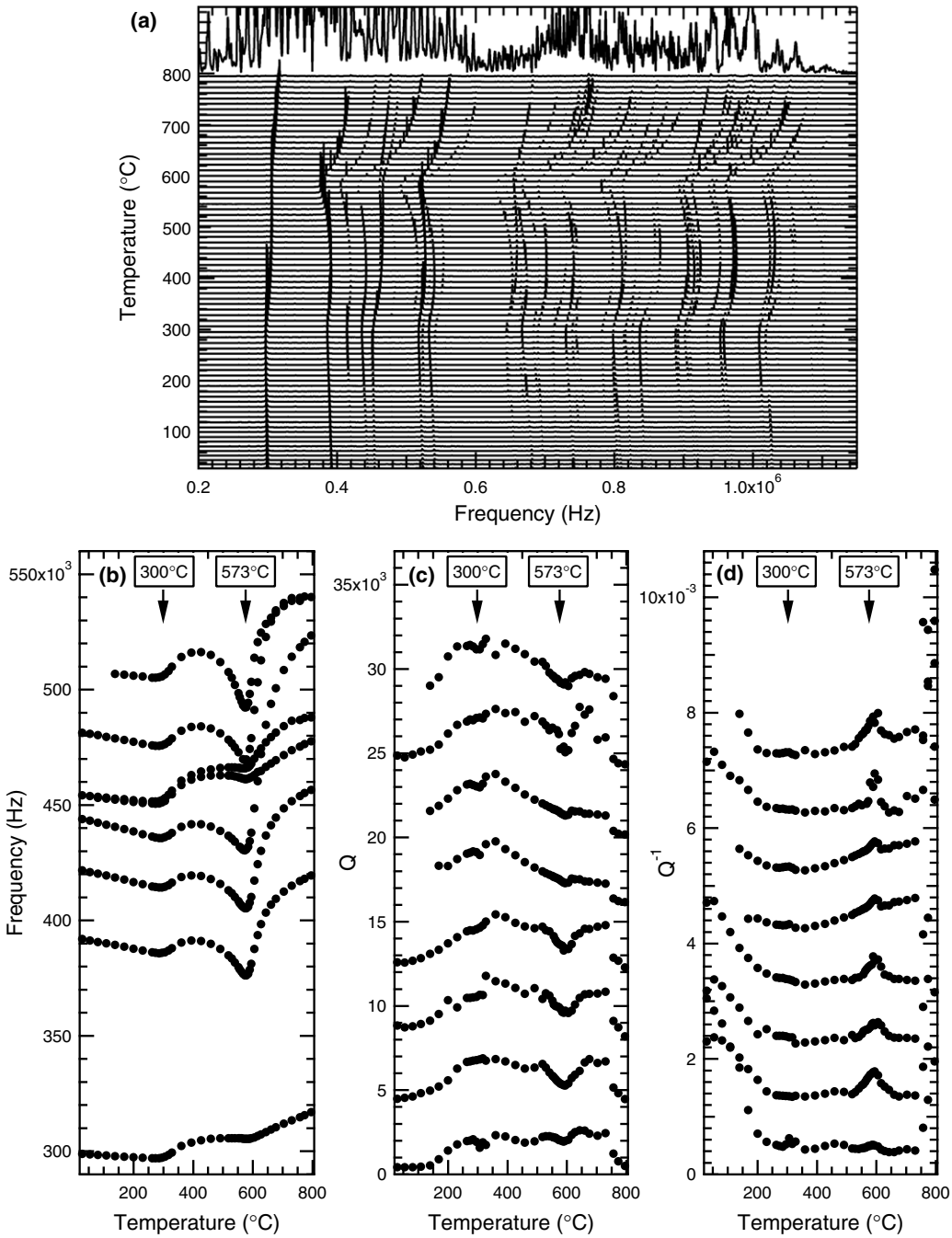

Figure 10. Data for Brazilian agate BR64 collected during heating from 29 to 795 °C. (a) RUS spectra in the frequency range 200–1150 kHz. The spectrum measured at 801 °C is shown at the top of the stack to illustrate the effect of the sample breaking and falling off the rods at some temperature between 795 and 801 °C. (b)–(d) Frequency, quality factor (Q), and inverse quality factor (Q^{-1}) variation respectively for 8 measurable peaks in the spectra shown in (a). Values of Q and Q^{-1} for each peak are offset from zero by different amounts for ease of inspection. The expected α–β transition temperature, at 573 °C, is marked in each figure with an arrow. The transition that is known to occur in moganite at ∼300 °C is also marked with an arrow.

softening in the vicinity of the transition temperature. However there is an unexpected softening of the moduli between ∼700 and 800 °C. Values for Ethiebeaton agate are systematically lower than the Hill averages for single crystal quartz from Ohno *et al* (2006) and Lakshtanov *et al* (2007), and also slightly lower than novaculite values.

In the cases of both Mexican and Brazilian agates, it was possible to measure the peaks across the full temperature range as they did not disappear in the vicinity of the phase transition. The fit for elastic constants for Mexican agate, based on the first ∼20 peaks, was very good across the whole temperature range (RMS error <1%) and values for both K and G were well constrained. The values obtained were comparable to single crystal values (see table 2), although not as close as for novaculite or Ethiebeaton agate. There are noticeable differences in the form of their elastic behaviour

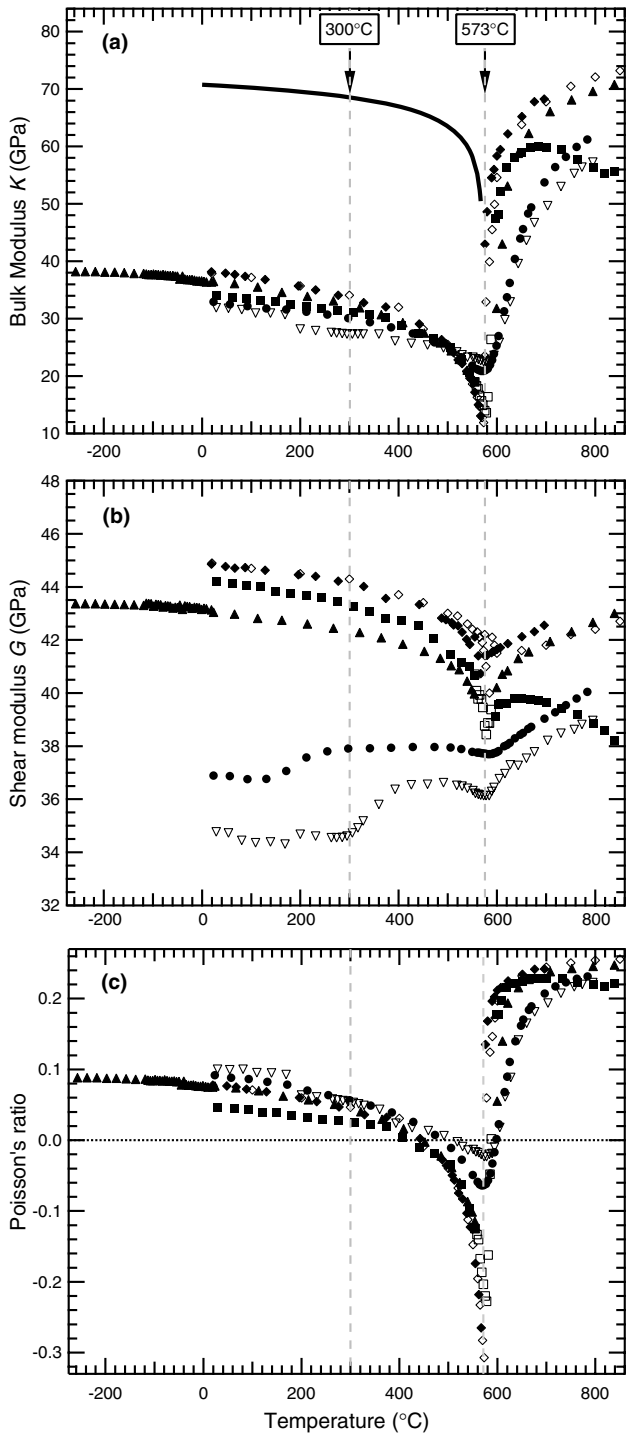

Figure 11. Evolution of (a) bulk modulus K, (b) shear modulus G and (c) Poisson's ratio for Brazilian agate BR64 (open triangles), Mexican agate MEX7a (closed circles), Ethiebeaton agate EQ12 (open and closed squares), and novaculite NOVC1 (closed triangles) during heating from room temperature. These are compared to Voigt/Reuss/Hill averages from single crystal data, as given by Ohno *et al* (2006) (closed diamonds) and Lakshtanov *et al* (2007) (open diamonds). The values for K calculated from the model of Pertsev and Salje (2000) for the nanocrystal limit are shown as a solid line in (a). The known α–β quartz transition at 573 °C and the moganite transition at 300 °C are marked with dashed lines. Note the difference in scales between (a) and (b): the K scale is 10–84 GPa, the G scale is much smaller at 32–48 GPa.

compared to single crystal quartz and the coarser grained polycrystalline samples (figures 11(b) and (c)). K shows a much less pronounced softening as the phase transition is approached and there is less recovery in the β-phase. G is clearly softer throughout the whole temperature range and shows an additional anomaly in the vicinity of 200 °C. In the vicinity of the α–β transition point, the amount of softening is also less than for the coarser grained samples.

The fit for elastic constants was quite poor in the case of the Brazilian agate, although still possible (RMS error = 2.3%). As in the case of the quartzite sample, this is probably due mainly to anisotropic distribution of grain sizes or grain orientations. The value for G was more tightly constrained by the data than the value for K. Fits for elastic moduli were carried out for the first 25–30 resonance peaks for high temperature spectra, using the fitted room temperature values (K = 36.9 GPa and G = 43.33 GPa) as starting estimates. The patterns of variation of both K and G (figures 11(a) and (b)) are essentially indistinguishable from those of the Brazilian agate, apart from the low temperature anomaly in G occurring at ∼300 °C rather than ∼200 °C.

Variations of Poisson's ratio calculated from the data in figures 11(a) and (b) are shown in figure 11(c.) Again, novaculite and Ethiebeaton agate show the same pattern of behaviour as single crystal quartz while Brazilian and Mexican agates differ. In particular, there is a region close to the transition temperature where Poisson's ratio becomes substantially negative for coarsely crystalline samples but remains positive or is only just negative for the fine grained agates.

5. Discussion

As predicted from the outset, there are clear differences according to grain size in how the elastic properties vary through the α–β phase transition as a function of temperature. Three different regimes, in terms of elastic behaviour, have been identified. Firstly, there is a grain size above which grains pull apart or crack, and below which polycrystalline samples remain coherent. Secondly, there is an intermediate region where the elastic properties are essentially those of single crystal quartz, though the transition temperature may be raised. Finally, there is a critical grain size between ∼120 and ∼65 nm below which the elastic properties start to differ from those of single crystal quartz. These effects do not appear to depend on water content of the samples, and could be due to stress/strain variations with grain size of the type illustrated schematically in figure 1. The limiting behaviour of strain and elastic constant variations for elastically clamped nanocrystals is not reached, however, and some of the observed variations appear to be associated with the presence of moganite.

Anisotropic thermal expansion causes a build up of stresses between and within grains in a polycrystalline material because the grains differ in crystallographic orientation. In the vicinity of the α–β quartz transition there is a marked increase in volume expansion, and anisotropic shear stresses are also likely to increase (see high temperature lattice parameter data in Carpenter *et al* (1998), for example). For relatively large

grain sizes, such stresses may ultimately be accommodated by pulling apart of grain boundaries or by cracking within grains. Direct evidence of this is provided by acoustic emissions from quartz bearing rocks when they are heated, with a strong peak of microcracking at the α–β transition temperature (Schmidt-Mumm 1991, Glover *et al* 1995, Meredith *et al* 2001). Development of microcracks would explain the substantial and irreversible change in RUS spectra observed for the quartzite sample (100–300 μm grain size) investigated here on heating above 573 °C.

Application of a confining pressure prevents microcracking in polycrystalline samples but also gives transition temperatures which are higher than expected from the pressure dependence of the transition point for single crystals (Kern 1979, 1982, Van der Molen 1981). This situation is represented by the cartoons of large and intermediate sized crystals in figure 1. Unrelaxed stresses within a grain act to raise its transition temperature beyond what is expected from the effect of the external pressure alone. At 0.2 GPa confining pressure the difference is ~25 °C (Kern 1979). Quartz grains in novaculite (1–5 μm grain size) evidently do not pull apart or crack, showing that there is a grain size limit for mechanical failure which is between ~5 and ~100 μm. An increase in the transition temperature of 7 °C above that of single crystal quartz corresponds to an internal pressure of 0.027 GPa using the pressure dependence of 256 °C GPa^{-1} given by Shen *et al* (1993).

Absolute values of the bulk and shear moduli of agate and novaculite are smaller than the Voigt/Reuss/Hill averages from single crystal data (table 2, figure 11). This is due, at least in part, to differences in density. Taking the densities for novaculite and single crystal quartz from table 2 leads to an estimate of 1.4% porosity in the novaculite sample. Using the correction procedure given by Ledbetter *et al* (1994) then gives $K = 37.8$ GPa and $G = 44.7$ GPa for novaculite with zero porosity at room temperature. These values are essentially indistinguishable from the single crystal data of Ohno *et al* (2006) and Lakshtanov *et al* (2007).

A second order transition ($Q^2 \propto (T_c - T)$) is expected to give a simple step in selected elastic constants at the transition point (T_c) for a co-elastic transition, with little variation below T_c (Slonczewski and Thomas 1970, Rehwald 1973, Carpenter and Salje 1998). The more nearly constant values of K below the transition point for fine grained agates, in comparison with the steep softening of single crystal and coarse polycrystalline samples, are thus qualitatively consistent with the suggestion of Pertsev and Salje (2000) that the transition becomes second order due to the increasing dominance of grain boundary effects. However, other more quantitative aspects of the observed changes in behaviour do not match up with the limiting case of fine grain sizes given by Pertsev and Salje (2000). In particular, there is no direct evidence for suppression of strain/order parameter coupling in the observed spontaneous strains for agates with grain sizes of ~90 nm (figures 2(b)) and (c); data of (Ríos *et al* 2001), and there is no sign of the substantial change in bulk modulus which should accompany this suppression (figure 11(a)). There is also no evidence for the transition temperature reducing to $T_c = 567$ °C as would be expected if the renormalized fourth order Landau coefficient, b^*, becomes positive. Rather, it appears that at grain sizes of ~50 nm quartz still retains its first order α–β transition at ~573 °C. In terms of the cartoon description of grain size effects in figure 1, 1–5 μm grains are perhaps represented by figure 1(b) while fine grained agates fall between figures 1(b) and (c), with at least partial stress relaxation such that the transition temperature is not increased. In this interpretation, the critical grain size for reducing to the homogeneous stress state of figure 1(c), and genuine 'nano' properties, is below ~50 nm.

Superficially at least, it appears that the interval over which fine grained agates differ in their elastic properties from coarse grained quartz is related to the interval over which single crystal quartz develops a negative Poisson's ratio Kern (1979), and figure 11(c)). Most materials have a positive Poisson's ratio and this correlates with a tendency for them to undergo elastic shear deformation but resist volume deformation. Materials with a negative Poisson's ratio undergo volume deformation but are stiffer with respect to shear deformation (Lakes 1987, Kimizuka and Kaburaki 2005). The implication is that the capacity for quartz to undergo elastic volume deformation is substantially reduced for grain size below ~50 nm, in comparison with larger crystals. That this difference is also restricted to an interval of only ~150 °C below the transition point further suggests that the change in behaviour is related to the build up of stresses in the sample associated with anisotropic thermal expansion. The transition temperature is not raised in these samples but seems to become somewhat smeared, and the discontinuity in K and G is lost, as might occur if the stress distribution is quite inhomogeneous. By way of contrast, the bulk modulus of β-quartz in fine grained samples is actually smaller than it is for coarser grains (figure 11(a)). No real explanation is offered for this behaviour here, but it should be noted that fine grained quartz samples show strong tails above the transition point in the evolution of lattice parameters (Sorrell *et al* 1974, Ríos *et al* 2001), heat capacity (Ríos *et al* 2001) and second-harmonic generation (Ríos *et al* 2001). In addition to the possible contribution of defects, the role of inhomogeneous stresses through grain boundaries and across distances of several tens of nanometres needs to be investigated in this context.

The moganite content of Mexican agate is ~11% and of Brazilian agate is ~21%. Both show elastic anomalies in the temperature interval at which structural changes accompanying a phase transition, *Imab–I2/a*, have been reported by Heaney and Post (2001) and Heaney *et al* (2007). Given that the transition involves predominantly the development of shear strain, associated anomalies in the elastic constants are likely to appear most strongly in the shear modulus. This is indeed the case for the Brazilian agate in the vicinity of 300 °C (figure 11(b)). An additional step in both K and G is present between 170 and 200 °C, however, and this correlates with a distinct break in slope of the evolution of unit cell volume shown in figure 4 of Heaney and Post (2001) and figure 9 of Heaney *et al* (2007). Heaney *et al* (2007) discuss the possibility that there might be a field of stability for some intermediate structure at this phase transition and the observation of two distinct elastic anomalies is consistent with this view. Only one

anomaly is seen in the data for Mexican agate, and although it is similar in form to the higher temperature (∼300 °C) anomaly of Brazilian agate, it occurs at ∼200 °C. Speculation as to the origin of this difference would not be justified without some better characterization of grain size and distribution of moganite in the two samples. It is also possible that some of the variations in K, in comparison with predictions from single crystals, are due to the presence of moganite dispersed along grain boundaries.

Acoustic dissipation in all the samples investigated is highly variable. A more or less reproducible peak in Q^{-1} occurs at the α–β transition point but there are also broad peaks at lower temperatures. Ferris and Martin (1994) have shown that anelastic relaxation of alkali ions in quartz can give rise to significant dissipative effects. A mixture of impurity ions is likely to be present in small concentrations in natural samples and these could contribute to the broad and irregular anelastic behaviour. Protons are also present and might also be involved in anelastic motions at frequencies which depend on their binding energies. Dissipation (Q^{-1}) associated explicitly with the transition point is restricted to a relatively narrow temperature interval of ∼100 °C for coarsely crystalline samples (figures 5(c), 7(c), 8(d)) but extends asymmetrically to lower temperatures for the fine grained agates (figures 9(d), 10(d)). The different evolution of K below the transition point in these samples presumably involves some contribution from anelastic effects, therefore. The behaviour of Dauphiné or Brazil twins in nanocrystalline quartz might be relevant in this context.

Acknowledgments

Ruth E A McKnight was supported by a studentship from the Engineering and Physical Sciences Research Council (grant no. EPSRC DTG05 10026782). The RUS equipment was built with a grant from the National Environmental Research Council of Great Britain (grant no. NER/A/S/2000/01055), which is gratefully acknowledged. Thanks go to Ekhard Salje for his comments on the manuscript, Juergen Schreuer for help with preliminary data collection, Brad Cross for kindly providing the Mexican agate, Bill Wilson for the Ethiebeaton agate, Geoff Lloyd for the quartzite sample, and Susana Ríos for lattice parameter data from her 2001 paper. Michael Carpenter and Terry Moxon thank The Leverhulme Trust for financial support of the agate studies.

References

Carpenter M A 2006 *Am. Mineral.* **91** 229–46
Carpenter M A and Salje E K H 1998 *Eur. J. Mineral.* **10** 693–812
Carpenter M A, Salje E K H, Graeme-Barber A, Wruck B, Dove M T and Knight K S 1998 *Am. Mineral.* **83** 2–22
Cummins H Z 1983 Brillouin scattering studies of phase transitions in crystals *Light Scattering Near Phase Transitions* ed H Z Cummins and A P Levanyuk (Amsterdam: North-Holland) pp 359–447
Eshelby J D 1957 *Proc. R. Soc.* A **241** 376–96
Ferris J E and Martin J J 1994 *Proc. 1994 IEEE Int. Frequency Control Symp.* pp 115–121
Fleury P A and Lyons K 1981 Optical studies of structural phase transitions *Structural Phase Transitions I* (*Springer Topics in Current Physics* vol 23) ed K A Muller and H Thomas (Berlin: Springer) pp 9–92
Glover P W J, Baud P, Darot M, Meredith P G, Boon S A, LeRavalec M, Zoussi S and Reuschlé T 1995 *Geophys. J. Int.* **120** 775–82
Heaney P J, McKeown D A and Post J E 2007 *Am. Mineral.* **92** 631–9
Heaney P J and Post J E 1992 *Science* **255** 441–3
Heaney P J and Post J E 2001 *Am. Mineral.* **86** 1358–66
Kassing R, Petkov P, Kulisch W and Popov C 2006 *Functional Properties of Nanostructured Materials* (*NATO Science Series II: Mathematics, Physics and Chemistry*) (Berlin: Springer)
Keller W D, Stone C G and Hoersch A L 1985 *Geol. Soc. Am. Bull.* **96** 1353–63
Keller W D, Viele G W and Johnson C H 1977 *J. Sed. Petrol.* **47** 834–43
Kern H 1979 *Phys. Chem. Mineral.* **4** 161–71
Kern H 1982 *Phys. Earth Planet. Inter.* **29** 12–23
Kimizuka H and Kaburaki H 2005 *Phys. Status Solidi* b **242** 607–20
Lakes R S 1987 *Science* **235** 1038–9
Lakshtanov D L, Sinogeikin S V and Bass J D 2007 *Phys. Chem. Mineral.* **34** 11–22
Ledbetter H, Lei M, Hermann A and Sheng Z 1994 *Physica* C **225** 397–403
Leisure R G and Willis F A 1997 *J. Phys.: Condens. Matter* **9** 6001–29
Lüthi B and Rehwald W 1981 Ultrasonic studies near structural phase transitions *Structural Phase Transitions I* (*Springer Topics in Current Physics* vol 23) ed K A Muller and H Thomas (Berlin: Springer) pp 131–84
Maynard J D 1996 *Phys. Today* **49** 26–31
McKnight R E A, Carpenter M A, Darling T W, Buckley A and Taylor P A 2007 *Am. Mineral.* **92** 1665–72
Meredith P G, Knight K S, Boon S A and Wood I G 2001 *Geophys. Res. Lett.* **28** 2105–8
Migliori A, Darling T W, Baiardo J P and Freibert F 2001 *Resonant Ultrasound Spectroscopy (RUS)* (*Handbook of Elastic Properties of Solids, Liquids, and Gases* vol 1) ed M Levy, H Bass and R Stern (New York: Academic) pp 239–62
Migliori A and Maynard J D 2005 *Rev. Sci. Instrum.* **76** 121301
Migliori A and Sarrao J L 1997 *Resonant Ultrasound Spectroscopy: Applications to Physics, Material Measurements and Nondestructive Evaluation* (New York: Wiley)
Migliori A, Sarrao J L, Visscher W M, Bell T M, Lei M, Fisk Z and Leisure R G 1993 *Physica* B **183** 1–24
Moriarty P 2001 *Rep. Prog. Phys.* **64** 297–381
Moxon T 2002 *Eur. J. Minerals* **14** 1109–18
Moxon T and Ríos S 2004 *Eur. J. Mineral.* **16** 269–78
Ohno I, Harada K and Yoshitomi C 2006 *Phys. Chem. Minerals* **33** 1–9
Pertsev N A and Salje E K H 2000 *Phys. Rev.* B **61** 902–8
Raz U, Girsperger S and Thompson A B 2003 *Schweiz. Min. Petrog. Mitt.* **83** 173–82
Rehwald W 1973 *Adv. Phys.* **22** 721–55
Ríos S, Salje E K H and Redfern S A T 2001 *Eur. Phys. J.* B **20** 75–83
Schmidt-Mumm A 1991 *Phys. Chem. Minerals* **17** 545–53
Schreuer J and Haussühl S 2005 *EMU Notes on Mineralogy* **7** 1–42
Schreuer J, Hildmann B and Schneider H 2006 *J. Am. Ceram. Soc.* **89** 1624–31
Schreuer J and Thybaut C 2005 *Proc. IEEE Ultrason. Symp. 2005* pp 695–8
Schreuer J, Thybaut C, Prestat M, Stade J and Haussühl S 2003 *Proc. IEEE Ultrason. Symp. 2003* pp 196–9
Shen A H, Bassett W A and Choiu I-M 1993 *Am. Mineral.* **78** 694–8
Slonczewski J C and Thomas H 1970 *Phys. Rev.* B **1** 3599–608
Sorrell C A, Anderson H U and Ackermann R J 1974 *J. Appl. Crystallogr.* **7** 468–73
Van der Molen I 1981 *Tectonophysics* **73** 323–42
Watt J P and Peselnick L 1980 *J. Appl. Phys.* **51** 1525–31